Delft University of Technology

Multimaterial control of instability in soft mechanical metamaterials

Janbaz, Shahram; McGuinness, Molly; Zadpoor, Amir A.

Important note
To cite this publication, please use the final published version (if applicable).
Please check the document version above.

Multimaterial Control of Instability in Soft Mechanical Metamaterials

Shahram Janbaz,[1,*] Molly McGuinness,[1,2] and Amir A. Zadpoor[1]

[1]*Department of Biomechanical Engineering, Faculty of Mechanical, Maritime,
and Materials Engineering, Delft University of Technology (TU Delft),
Mekelweg 2, 2628 CD, Delft, Netherlands*
[2]*Department of Biomedical Engineering, University of Glasgow,
University Road, G12 8QQ, Glasgow, United Kingdom*

Soft mechanical metamaterials working on the basis of instability have numerous potential applications in the context of "machine materials." Controlling the onset of instability is usually required when rationally designing such metamaterials. We study the isolated and modulated effects of geometrical design and material distribution on the onset of instability in multimaterial cellular metamaterials. We use multimaterial additive manufacturing to fabricate cellular specimens whose unit cells are divided into void space, a square element, and an intermediate ligament. The ratio of the elastic modulus of the ligament to that of the square element $[(E_L)/(E_S)]$ is changed by using different material types. Computational models are also developed, validated against experimental observations, and used to study a wide range of possible designs. The critical stress can be adjusted independently from the critical strain by changing the material type while keeping $[(E_L)/(E_S)]$ constant. The critical strain shows a power-law relationship with $[(E_L)/(E_S)]$ within the range $[(E_L)/(E_S)] = 0.1–10$. The void shape design alters the critical strain by up to threefold, while the combined effects of the void shape and material distribution cause up to a ninefold change in the critical strain. Our findings highlight the strong influence of material distribution on the onset of the instability and buckling mode.

I. INTRODUCTION

Mechanical metamaterials [1,2] are usually designed to exhibit unusual mechanical behavior such as negative [3,4] or ultrahigh [5] values of mechanical properties. Most mechanical metamaterials are architectured [6], meaning that their large-scale properties originate from the design of their small-scale architecture. Rational design [7] techniques based on computational and analytical models are often used to devise the small-scale architectures that give rise to the desired set of mechanical properties. The geometrical basis for designing such architectures may be lattice structures [5,8,9], origami [7,10,11], or kirigami [12–14], among others.

The very concept of "architectured" metamaterials implies the presence of more than one material, as geometrical patterns, particularly those relevant for metamaterial design, generally require at least two types of material properties. In cellular or lattice structures, those materials include the matrix material with finite properties and the "voids" with negligibly low properties. The rational design of cellular structures then reduces to devising a plan for spatially distributing the matrix material and leaving the remainder of the space for the voids. Milton and Cherkaev have shown that any thermodynamically admissible elasticity tensor can be realized by combining a matrix material with a void material [15]. When dealing with large deformations of soft matter, the void material plays an important role in guiding the deformation path. The soft metamaterials working on the basis of buckling instability [16–18] are perhaps the best examples for showcasing the role of the voids. Voids enable local buckling, control the instability threshold, and guide the postbuckling behavior of such materials [19–21].

Additive manufacturing has enabled arbitrarily complex spatial distributions of the matrix and void materials for several years. Recent advances in multimaterial additive manufacturing techniques have, however, enabled us to go much further and spatially distribute practically an unlimited number of materials in a single-step manufacturing process, thereby opening many novel avenues for the design of architectured materials [22]. In this study, we explore how the spatial distribution of multiple materials can be used to rationally design soft cellular metamaterials that work on the basis of buckling instability. Those materials have numerous potential applications in the context of "machine materials" [23,24] that span areas as diverse as soft robotics, flexible

*Corresponding author.
s.janbaz@tudelft.nl

electronics, and medical implants. In particular, we consider multiple void geometries and different types of material distributions to study the isolated and modulated effects of geometrical design and material combination on the instability behavior of such materials.

II. MATERIALS AND METHODS

The cellular structures are based on square unit cells whose void geometry is described using the following relationship [20]:

$$V(\theta) = c[(1+r) - d(-1)^{(n+2)/2}(r-1)\cos(n\theta)], \quad (1)$$

where $c = [\sqrt{2\pi(3 + 3r^2 + 2r)\phi}P]/[\pi(3 + 3r^2 + 2r)]$, $0 \leq \theta \leq 2\pi$, ϕ denotes the void fraction per unit-cell area, r determines the fold sharpness, $d = \pm 1$ defines the xy symmetry style, n regulates the number of folds, and P is the length of the unit cell. Three types of void shapes including a circular $[(\phi, r, d, n) = (0.45, -, -, -)]$, fourfold type 1 $[(\phi, r, d, n) = (0.45, 0.7, +1, 4)]$, and fourfold type 2 $[(\phi, r, d, n) = (0.45, 0.7, -1, 4)]$ are considered (Fig. 1).

The unit cells are partitioned symmetrically into ligaments and square-shaped elements [Fig. 1(a)]. Three different ratios of ligament length a and square sides b are considered: $(a/b) = \frac{4}{6}, \frac{5}{5}, \frac{6}{4}$. For each of the three void shapes,

two different types of specimens [Fig. 1(d)] are additively manufactured using a multimaterial 3D printer (Stratasys Objet 350 Connex3, U.S.) that works on the basis of jetting UV-curable photopolymers. During the printing process, all specimens are oriented such that the printing direction is in parallel with the loading direction. In the first series of specimens, the ligament material (TangoPlus, nominal shore hardness $A = 27$) is softer than the square material (digital combination of Vero and TangoPlus, nominal shore hardness $A = 60$). The opposite is held for the ligament (digital combination of Vero and Agilus, nominal shore hardness $A = 60$) and square (Agilus, nominal shore hardness $A = 30$) materials in the second set of specimens. The specimens include 8×8 crosslike unit cells and are designed with equal lengths of the ligament and square (i.e., $(a/b) = \frac{5}{5}$). Two hard clamps (Vero) are printed at both ends of the specimens to ensure consistent load application. A nominal unit-cell length P of 10 mm and an out-of-plane thickness of 15 mm are considered for the design of the specimens. The specimens are mechanically tested under compression using a Lloyd test bench (LR5K) equipped with a 100-N load cell. A constant deformation rate of 1 mm/ min is used. Two acrylic plates are placed on both sides of the specimens to preserve the plane strain conditions. Both sides of the specimens are polished and sprayed with a lubricant (Multi Spray 1000, Innotec) to minimize their friction with the acrylic plates. A digital camera (Sony a7R with a Sony FE 90 mm f/2.8 macro OSS lens) captures the deformations of the specimens during the mechanical tests. In addition, tensile strips with rigid rectangular end clamps are produced to obtain an initial estimation of the mechanical properties of the different types of polymers used in this study. A neo-Hookean hyperelastic model is fitted to the results of the tensile test experiments and fine-tuned using the results of the compression tests. The following material parameters are obtained: $C_{10}^{\text{soft}} = 0.13$ MPa, $C_{10}^{\text{hard}} = 0.23$ MPa for the first series of specimens and $C_{10}^{\text{soft}} = 0.07$ MPa, $C_{10}^{\text{hard}} = 0.20$ MPa for the second series of specimens. The superscripts "soft" and "hard" refer to the softest and hardest materials among the ligament and square materials.

The instability behavior of the designed metamaterials is also analyzed computationally. The computational models are first validated against the experimental results and are then expanded to analyze the effects of material choice and (a/b) values on the instability behavior of the specimens. The geometry of the computational models includes 8×8 unit cells and is discretized using six-node triangular hybrid plane strain elements (CPE6H, Abaqus/Standard). The polymers are considered to be nearly incompressible. The computational models are solved using an implicit solver (Abaqus/Standard, version 6.13). The full Newton's method is used (default option) as a solution technique in Abaqus/Standard. A convergence study is performed to determine the size of the elements, resulting in an average density of 995
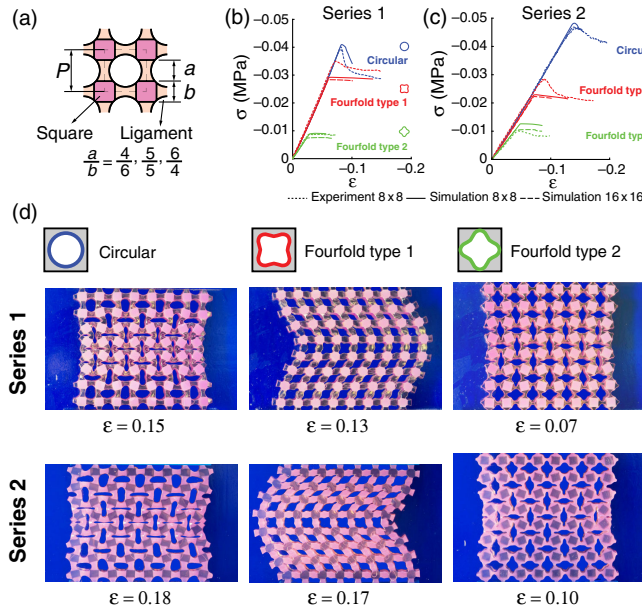

FIG. 1. (a) The geometry of the unit cells used in the design of the metamaterials and the division of the unit cells into ligaments and square elements. (b),(c) Comparison between experimentally determined and computationally predicted stress-strain curves for two different combinations of material properties and three different void shapes. (d) The instability modes of two different types of multimaterial metamaterials with three different void shapes. Series 1 and 2 represent the structures in which the ligament material is softer and stiffer than the square material, respectively.

to 1017 elements per unit cell. The buckling modes are determined using linear buckling analysis, and a small imperfection of 0.01 from the buckling analysis is introduced into the models. The top and bottom nodes of the models are constrained to move together with their respective reference points, thereby ensuring consistent deformation of the clamped nodes. The elastic modulus E and neo-Hookean material parameter C_{10} for an incompressible elastomer are assumed to be related through the following relationship: $E = 6C_{10}$ (because of the consistency with linear elasticity $G = 2C_{10}$ in which G is the initial shear modulus of hyperelastic rubber and the relationship $E = 3G$). Five different ratios of the elastic modulus of the ligament material E_L to that of the square material E_S within the range of 0.1 to 10 are considered for performing the instability analyses. To evaluate whether a computational analysis with 8×8 unit cells is sufficient to predict the behavior of cellular structures with a larger number of unit cells, additional analyses are performed using 16×16 unit cells.

III. RESULTS AND DISCUSSION

The onset of instability can be clearly seen as a local maximum in the stress-strain curves of the specimens from both categories [Figs. 1(b) and 1(c)]. The instability patterns of all specimens are either compaction or side buckling [Fig. 1(d)]. For all designs, the computational models can accurately predict the linear part of the stress-strain curve, the onset of instability, and the type of instability [Figs. 1(b) and 1(c)]. The analysis with 16×16 unit cells confirms that the use of 8×8 cellular structures is sufficient to predict the behavior of cellular structures with a larger number of unit cells [Figs. 1(b) and 1(c)]. For all void shapes, the critical strain is higher when the ligament material is harder than the square material (i.e., the critical strains are higher in the second series of the specimens compared to the first series) [Figs. 1(b) and 1(c)]. Numerically estimated maximum stress and the critical strain values for the structures with the void shape of fourfold type 1, regardless of the ratio $[(E_L)/(E_S)]$, deviates from those observed in the experiments [Figs. 1(b) and 1(c), the stress-strain curves highlighted in red]. The mismatch between the numerical and experimental results may be partly attributed to the friction between the samples and acrylic plates preventing out-of-plane buckling, use of an idealized material model in simulations without consideration of imperfection from production process, but mismatch is expected to be mainly due to viscosity effects during the fast pattern transformation coincident with the onset of instability. The geometrical design of the experimentally studied structures with fourfold type 1 voids results in general buckling (i.e., side buckling) happening with faster deformation rates compared to the two other types of structures. Viscosity consequently resists the rapid pattern transformation and postpones the occurrence of peak in the stress-strain curves and increases the strain at
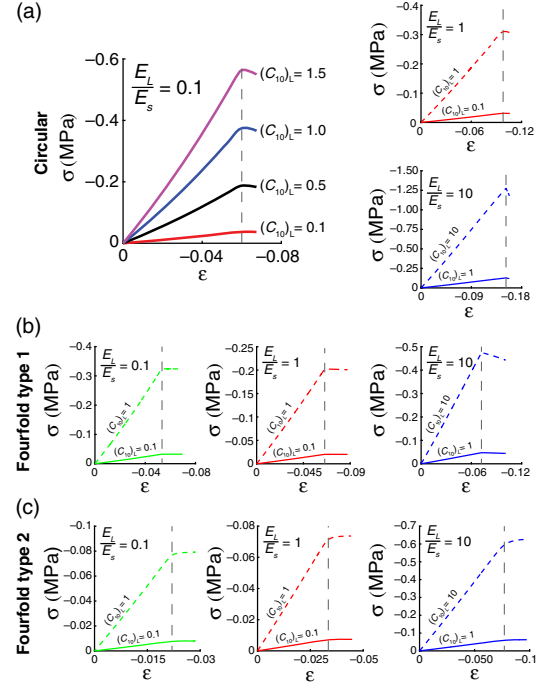

FIG. 2. The stress-strain curves of metamaterials based on circular (a), fourfold type 1 (b), and fourfold type 2 (c) void shapes. The different values of the elastic modulus do not change the critical strain as long as $[(E_L)/(E_S)]$ remains constant. Critical stresses are, however, scaled by the changes in the absolute values of the elastic moduli.

which the local maximum stress happens [see the red curves in Figs. 1(b) and 1(c)].

Computational analyses show that as long as the ratio of the elastic modulus of the ligament material to that of the square material $[(E_L)/(E_S)]$ is constant, the critical strain remains constant regardless of the absolute values of the elastic modulus of both materials (Fig. 2). That same observation holds for all types of void shapes and for all considered values of $[(E_L)/(E_S)]$ between 0.1 and 10 (Fig. 2). The only difference is the altered critical stress values, i.e., the stress values at which instability commences (Fig. 2). This implies that the critical stress values can be adjusted independently from the critical strain simply by changing the absolute values of the material properties while keeping their ratio constant. From the practical viewpoint, the multimaterial additive manufacturing technique used here allows for a combination of up to three materials at the voxel level to achieve several hundreds of different material properties. It is, therefore, perfectly feasible to change the absolute values of the material properties while satisfying additional constraints such as a constant $[(E_L)/(E_S)]$ value.

The critical strain of the metamaterial increases with $[(E_L)/(E_S)]$, while the ratio of the elastic modulus of the metamaterial to that of the ligament material $[E^*/(E_L)]$ decreases with $[(E_L)/(E_S)]$ (Fig. 3). In the range of $[(E_L)/(E_S)]$ values between 0.1 and 10, the trend line of
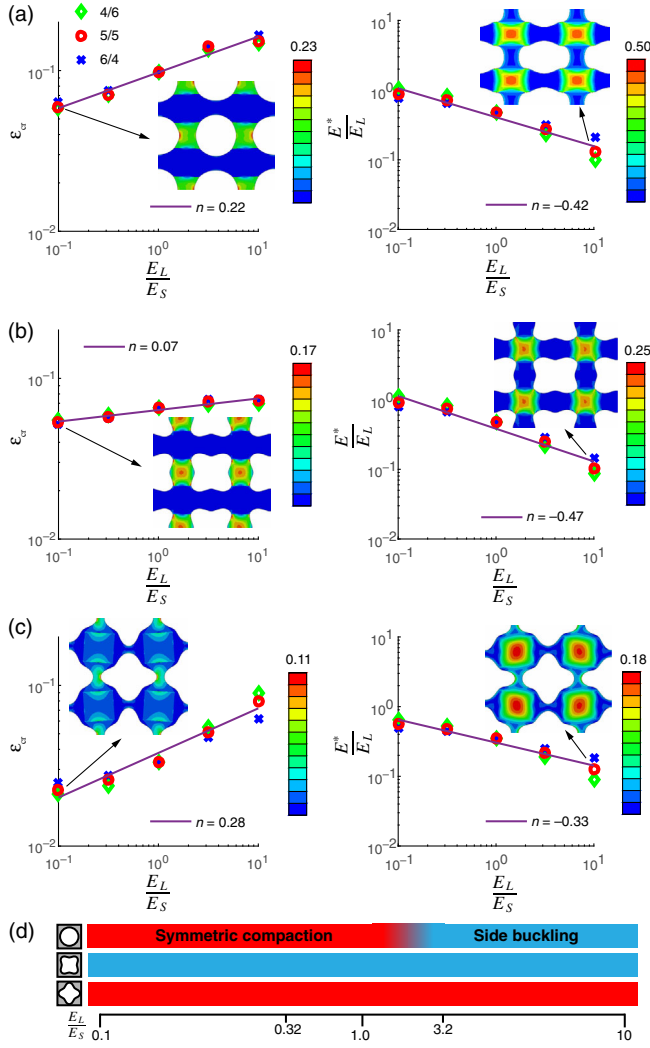
FIG. 3. The critical strain and normalized elastic modulus of the metamaterials based on circular (a), fourfold type 1 (b), and fourfold type 2 (c) void shapes. The strain distributions are also depicted for the smallest and largest $[(E_L)/(E_S)]$ values. The instability modes for different void shapes are presented in (d). The color ramp highlights the influence of geometrical imperfection in the transition from symmetric compaction to side buckling in metamaterials with circular voids.

the changes in the critical strain and $[E^*/(E_S)]$ can be described using a power law (Fig. 3). The power-law exponents are different for the different void shapes considered here. While studying the change in the critical strain, the fourfold type 2 shows the highest power-law exponents, and the fourfold type 1 shows the lowest exponents (Fig. 3). This suggests that geometrical features such as void geometry modulate the effects of material distribution on the critical strain of multimaterial metamaterials. The plots in Figs. 3(a)–3(c) show the strain distributions in four unit cells at the middle part of each structure for the lowest and highest values of $[(E_L)/(E_S)]$. The contours indicate that the vertical ligaments, the

vertical ligaments aligned along the compressive load directions, experience high strain when the stiffness of the ligaments is considerably lower than the squares $([(E_L)/(E_S)] = 0.1)$. In contrast, the squares experience high strains when the ligaments are stiffer. However, the results for the structures with fourfold type 2 voids illustrate that the slenderness of the ligaments can highly influence the level of strains in the ligaments even when the ligaments are stiffer than the squares. The Supplemental Material Videos V1–V3 [25] display the strain evolution and the precedence of instability in the studied structures while $[(E_L)/(E_S)] = 0.1, 1.0, 10$. When the shape of the ligaments can preserve the mode of buckling in the structures with voids fourfold types 1 and 2 (i.e., respectively, side buckling and symmetric compaction), increasing the stiffness ratio $([(E_L)/(E_S)])$ can transform the mode of buckling from symmetric compaction to side buckling in the structures with circular voids. Figure 3(d) depicts the buckling modes for the given ratios of material properties $([(E_L)/(E_S)] = 0.1, 0.32, 1, 3.2, 10)$ and void shapes. The influence of geometrical imperfection in the transition from symmetric compaction to side buckling in the structures with circular voids is proposed in the form of a color ramp in Fig. 3(d).

Quantitatively speaking, void shape alone can change the critical strain by up to threefold, while up to ninefold difference in the critical strain is achieved when the effects of void shape are combined with those of material distribution.

To better understand the changes in the critical strain with $[(E_L)/(E_S)]$, we use the first-order approximations available from the linear theory of stability [26,27]. There are two competing modes of instability, namely, symmetric compaction and side buckling. Symmetric compaction is caused by the buckling of individual ligaments and is, thus, a specific type of local buckling. Side buckling, on the other hand, is the global buckling of the cellular structures as a whole.

The critical load of individual ligaments is given by

$$P_{cr,L} = \frac{\pi^2 E_L w^3 t}{12(k_L a)^2}, \qquad (2)$$

where w is the equivalent width of the ligament, t is the thickness of the ligament, a is the length of the ligament, and k_L is a factor dependent on the boundary conditions.

The critical load of the entire cellular structure per unit cell P_{cr}^* is

$$P_{cr}^* = \frac{\pi^2 E^* L^3 t}{n12(k^* L)^2}, \qquad (3)$$

where L is the length of the cellular structure, E^* is the elastic modulus of the cellular structure, t is the thickness of the cellular structure, n is the number of the unit cells along

each edge of the specimen, and k^* is a factor dependent on the boundary conditions of the cellular structure.

Replacing $n = 8$ and $L = 16a$ in Eq. (3) and assuming $k_L \approx k^*$, the ratio of the side-buckling critical load P^*_{cr} to that of symmetric compaction $P_{cr,L}$ can be written as

$$\frac{P^*_{cr}}{P_{cr,L}} \approx 2\left(\frac{E^*}{E_L}\right)\left(\frac{a}{w}\right)^3. \qquad (4)$$

It can, therefore, be concluded that either side buckling or symmetric compaction can occur depending on the stiffness of the cellular structure as compared to that of the ligament and the shape of the voids. Considering the fact that for the circular void shapes $w \approx a$ for fourfold type 1 $w > a$ (due to the barrel-like shape of the ligaments), and for fourfold type 2, $w \ll a$ (due to the cutouts in the ligaments) and replacing for $[E^*/(E_L)]$ from the values found in Fig. 3, we find that the predicted buckling modes based on Eq. (4) are in agreement with those found computationally [Fig. 3(d)]. To put Eq. (3) in perspective, the term $(a/w)^3$ represents the effects of the geometrical design on the onset of the instability and instability mode. The cubic nature of this term highlights the strong effects that small changes in the geometrical design can have on the instability behavior of the metamaterial. The term $[E^*/(E_L)]$, on the other hand, represents the effects of material distribution on the instability behavior. The power-law relationship between $[(E_L)/(E_S)]$ and $[E^*/(E_L)]$ (Fig. 3) shows that the spatial distribution of the different materials can also strongly influence the instability behavior. As is clear from the different power-law exponents found for different void shapes, there are also modulations between the effects of geometrical design and those of material combination that cannot be captured by the simplified analytical models available from the linear theory of stability.

IV. CONCLUDING REMARKS

In summary, the presented design of multimaterial metamaterials allows for adjustment of both critical stress and critical strain. Critical stress can be changed independently from the critical strain by keeping the ratio of the elastic modulus of the ligament material to that of the square material constant while changing the absolute values of the elastic moduli. A power-law relationship between $[(E_L)/(E_S)]$ and critical strain is found for $[(E_L)/(E_S)]$ values between 0.1 and 10. We also find that geometrical features such as void geometry not only affect the critical strains themselves but also modulate the effects of the parameters describing material distribution (e.g., $[(E_L)/(E_S)]$ and a/b). To put those effects in perspective, geometrical features can change the critical strain up to threefold, while up to ninefold change in critical strain can be achieved by combining the effects of geometrical features with those of material distribution.

[1] J. H. Lee, J. P. Singer, and E. L. Thomas, Micro-/nanostructured mechanical metamaterials, Adv. Mater. 24, 4782 (2012).

[2] A. A. Zadpoor, Mechanical meta-materials, Mater. Horizons 3, 371 (2016).

[3] B. Florijn, C. Coulais, and M. van Hecke, Programmable Mechanical Metamaterials, Phys. Rev. Lett. 113, 175503 (2014).

[4] Z. G. Nicolaou and A. E. Motter, Mechanical metamaterials with negative compressibility transitions, Nat. Mater. 11, 608 (2012).

[5] X. Zheng et al., Ultralight, ultrastiff mechanical metamaterials, Science 344, 1373 (2014).

[6] Y. Brechet and J. D. Embury, Architectured materials: Expanding materials space, Scr. Mater. 68, 1 (2013).

[7] J. T. Overvelde, J. C. Weaver, C. Hoberman, and K. Bertoldi, Rational design of reconfigurable prismatic architected materials, Nature (London) 541, 347 (2017).

[8] R. Hedayati, A. M. Leeflang, and A. A. Zadpoor, Additively manufactured metallic pentamode meta-materials, Appl. Phys. Lett. 110, 091905 (2017).

[9] L. R. Meza, S. Das, and J. R. Greer, Strong, lightweight, and recoverable three-dimensional ceramic nanolattices, Science 345, 1322 (2014).

[10] J. T. Overvelde, T. A. de Jong, Y. Shevchenko, S. A. Becerra, G. M. Whitesides, J. C. Weaver, C. Hoberman, and K. Bertoldi, A three-dimensional actuated origami-inspired transformable metamaterial with multiple degrees of freedom, Nat. Commun. 7, 10929 (2016).

[11] J. L. Silverberg, J.-H. Na, A. A. Evans, B. Liu, T. C. Hull, Christian D. Santangelo, R. J. Lang, R. C. Hayward, and I. Cohen, Origami structures with a critical transition to bistability arising from hidden degrees of freedom, Nat. Mater. 14, 389 (2015).

[12] T. Castle, Y. Cho, X. Gong, E. Jung, D. M. Sussman, S. Yang, and R. D. Kamien, Making the Cut: Lattice Kirigami Rules, Phys. Rev. Lett. 113, 245502 (2014).

[13] Bryan Gin-ge Chen, B. Liu, A. A. Evans, J. Paulose, I. Cohen, V. Vitelli, and C. D. Santangelo, Topological Mechanics of Origami and Kirigami, Phys. Rev. Lett. 116, 135501 (2016).

[14] A. Rafsanjani and K. Bertoldi, Buckling-Induced Kirigami, Phys. Rev. Lett. 118, 084301 (2017).

[15] G. W. Milton and A. V. Cherkaev, Which elasticity tensors are realizable?, J. Eng. Mater. Technol. 117, 483 (1995).

[16] S. Babaee, J. Shim, J. C. Weaver, E. R. Chen, N. Patel, and K. Bertoldi, 3D soft metamaterials with negative Poisson's ratio, Adv. Mater. 25, 5044 (2013).

[17] K. Bertoldi, P. M. Reis, S. Willshaw, and T. Mullin, Negative Poisson's ratio behavior induced by an elastic instability, Adv. Mater. 22, 361 (2010).

[18] J. T. B. Overvelde, S. Shan, and K. Bertoldi, Compaction through buckling in 2D periodic, soft and porous structures: Effect of pore shape, Adv. Mater. 24, 2337 (2012).

[19] B. Florijn, C. Coulais, and M. van Hecke, Programmable mechanical metamaterials: The role of geometry, Soft Matter 12, 8736 (2016).

[20] S. Janbaz, H. Weinans, and A. A. Zadpoor, Geometry-based control of instability patterns in cellular soft matter, RSC Adv. 6, 20431 (2016).

[21] J. T. B. Overvelde and K. Bertoldi, Relating pore shape to the non-linear response of periodic elastomeric structures, J. Mech. Phys. Solids **64**, 351 (2014).

[22] J. Hiller and H. Lipson, Tunable digital material properties for 3D voxel printers, Rapid Prototyping J. **16**, 241 (2010).

[23] C. Coulais, E. Teomy, K. de Reus, Y. Shokef, and M. van Hecke, Combinatorial design of textured mechanical metamaterials, Nature (London) **535**, 529 (2016).

[24] D. Yang, B. Mosadegh, A. Ainla, B. Lee, F. Khashai, Z. Suo, K. Bertoldi, and G. M. Whitesides, Buckling of elastomeric beams enables actuation of soft machines, Adv. Mater. **27**, 6323 (2015).

[25] See Supplemental Material at http://link.aps.org/supplemental/10.1103/PhysRevApplied.9.064013 for the evolution of strain patterns in multimaterial mechanical metamaterials.

[26] D. O. Brush and B. O. Almroth, *Buckling of Bars, Plates, and Shells* (Bull Ridge Publishing, Blacksburg, Virginia, 1975).

[27] S. P. Timoshenko and J. M. Gere, *Theory of Elastic Stability* (Dover Publications Inc., Mineola, New york, 1961).